PCCP

ROYAL SOCIETY OF CHEMISTRY

PAPER

View Article Online
View Journal | View Issue

Cite this: *Phys. Chem. Chem. Phys.*, 2021, **23**, 25256

DNA-mediated hierarchical organization of gold nanoprisms into 3D aggregates and their application in surface-enhanced Raman scattering†

Emtias Chowdhury,[a] Mohammad Shahinur Rahaman,[b] Noppadon Sathitsuksanoh,[b] Craig A. Grapperhaus[a] and Martin G. O'Toole *[c]

Colloidal crystallization using DNA provides a robust method for fabricating highly programmable nanoparticle superstructures with collective plasmonic properties. Here, we report on the DNA-guided fabrication of 3D plasmonic aggregates from polydisperse gold nanoprisms. We first construct 1D crystals *via* DNA-induced and shape-directed face-to-face assembly of anisotropic gold nanoprisms. Using the near-T_m thermal annealing approach that promotes long-range DNA-induced interaction and ordering, we then assemble 1D nanoprism crystals into a 3D nanoprism aggregate that exhibits a polycrystalline morphology with nanoscale ordering and microscale dimensions. The presence of closely packed nanoprism arrays over a large area gives rise to strong near-field plasmonic coupling and generates a high density of plasmonic hot spots within the 3D nanoprism aggregates that exhibit excellent surface-enhanced Raman scattering performance. The plasmonic 3D nanoprism aggregates demonstrate significant SERS enhancement ($<10^6$), and low detection limits (10^{-9}M) with good sample-to-sample reproducibility (CV ~ only 5.6%) for SERS analysis of the probe molecule, methylene blue. These findings highlight the potential of 3D anisotropic nanoparticle aggregates as functional plasmonic nanoarchitectures that could find applications in sensing, photonics, optoelectronics and lasing.

Received 10th August 2021,
Accepted 20th October 2021

DOI: 10.1039/d1cp03684j

rsc.li/pccp

1. Introduction

The ability of plasmonic nanoparticles to concentrate light into nanoscale volumes and create locally enhanced strong electromagnetic (EM) fields has been exploited for a broad array of applications such as optical antennae,[1,2] ultrasensitive sensors,[3–6] information processing,[7] surface-enhanced Raman scattering (SERS),[8–10] surface-enhanced fluorescence (SEF),[11,12] and nonlinear optics.[13] In particular, anisotropic-shaped nanoparticles (rods, prisms) such as those made of Au and Ag have been the subject of intense interest in surface-enhanced spectroscopies, for instance, SERS[10,14] and SEF,[15,16] because of their sharp edges and vertices that greatly confine the EM field, and the tunability of their surface plasmon resonance throughout the visible and near-IR (NIR) regions.[17–19] In addition, assembling such nanoparticles in a predesigned spatial arrangement with gap sizes of the order of a few nanometers leads to the formation of so-called plasmonic hot spots due to nanogap effects.[20,21] When a Raman reporter molecule or a fluorescence emitter is placed in those hot spots, strong SERS and SEF enhancement are observed due to strong near-field coupling between neighboring nanoparticles that induces an enormous EM field enhancement.[22,23] The strength of the EM field enhancement within the nanogap can be modulated by several key factors such as the gap distance, the particle shape/size, and the excitation configuration.[24] The concept of nanogap effects and the desirability of a high density of hot spots in the excitation laser focal volume has led to the development of various 2D and 3D nanoparticle superlattices with extensive plasmonic coupling to obtain large-area SERS hot spots.[25,26]

The assembly of nanoparticles into 3D nanostructures with tunable spacing provides a path towards the development of tailorable functional materials with collective properties.[27–29] In turn, these properties have been utilized for different applications including in magnetics,[30] plasmonics,[31] surface-enhanced spectroscopies,[32] photonics,[33] and optoelectronics.[34] The maximum utility of the nanoparticle arrangement towards the realization of novel nanomaterials depends upon the ability to control the orientation and spacing between the nanoparticles within the

[a] *Department of Chemistry, University of Louisville, Louisville, Kentucky 40292, USA*
[b] *Department of Chemical Engineering, University of Louisville, Louisville, Kentucky 40292, USA*
[c] *Department of Bioengineering, University of Louisville, Louisville, Kentucky 40292, USA. E-mail: martin.otoole@louisville.edu*

† Electronic supplementary information (ESI) available. See DOI: 10.1039/d1cp03684j

superstructures.[35,36] Common top-down and bottom-up strategies to fabricate plasmonic superstructures include electron beam lithography,[37,38] the Langmuir–Blodgett technique,[39] the droplet evaporation method,[40,41] interface-based assembly,[42] and the acoustic levitation technique.[43] All of these methods are either labor-intensive and costly or inefficient in terms of reproducibility and specificity.[44]

DNA nanotechnology approaches have emerged as a powerful route to form design-based nanostructures that enable a high degree of control over the placement of nanoparticles.[45–49] The programmability of the DNA length, recognition features, and binding specificity in complementary DNA interactions allow fine control in tuning the interparticle spacing, lattice symmetry, and nanoparticle composition.[50–52] These properties make the DNA-induced assembly of nanoparticles an ideal platform for developing well-defined 2D and 3D plasmonic nanostructures from both spherical and non-spherical nanoparticles.

Although the programmable DNA assembly has been used to create well-defined 3D arrangements of anisotropic nanoparticles (gold nanorods, cubes, rhomboids, and dodecahedra),[53–55] the formation of such nanostructures of anisotropic gold nanoprisms using DNA has not been reported. Herein, we demonstrate the stepwise hierarchical fabrication of 3D plasmonic aggregates from polydisperse anisotropic gold nanoprisms and their application as SERS substrates. Using DNA as the surface ligand and binding motif, prisms are organized into 1D crystals through preferential face-to-face binding, which maximizes the DNA interactions. By subjecting the 1D nanoprism crystals to extended annealing below the T_m of the crystals, micrometer-scale 3D plasmonic nanoprism aggregates composed of densely packed 1D nanoprism arrays are fabricated. The plasmonic activity and suitability of 3D plasmonic aggregates as SERS substrates are investigated. SERS analysis of the probe molecule methylene blue (MB) using 3D plasmonic aggregates demonstrates the excellent SERS enhancement.

2. Result and Discussion

Gold nanoprisms in the size range 100–200 nm were synthesized *via* the Diasynth method and purified following literature precedents.[5,56,57] The purified nanoprisms were densely functionalized with two complementary DNA strands, DNA-A and DNA-A′ (see ESI† for details). DNA-induced hierarchical assembly of the gold nanoprisms was accomplished in two steps: the DNA-functionalized nanoprisms were first assembled into 1D nanoprism arrays; these were then crystallized into 3D aggregates in the second step *via* long-range DNA-driven interactions of the 1D nanoprism stacks that were induced by thermal annealing.

Prisms are essentially 2D nano-objects with two extended flat surfaces that are significantly larger than their thickness. The assembly of nanoparticles preferentially occurs through binding events that allow maximum hybridization interactions between ligands anchored on the surface of the particles.[58] One can, therefore, assume that prisms having two large flat surfaces that can accommodate a high local ligand concentration will exhibit face-to-face stacking. In the DNA-mediated assembly of nanoparticles, in addition to shape complementarity, soft shells of DNA dictated by chain length and rigidity also play a crucial role in the orientational packing of anisotropic nanoparticles.[59,60] For instance, the length of DNA linkers can be used to control the DNA grafting density in different surface facets of anisotropic nanoparticles, facilitating the design of complex self-assembly schemes. A recent study by Gang and co-workers has demonstrated that short DNA chains tend to bind to the faces, whereas long DNA chains preferentially graft on high-curvature locations of anisotropic cubic nanoparticles.[61] Here, we designed small DNA shells by grafting short DNA linkers containing only 21 nucleotides to nanoprisms in order to ensure a maximum DNA grafting density on the flat surfaces of nanoprisms. Therefore, DNA-functionalized prisms are expected to preferentially bind in an associative manner *via* their large flat surfaces.

When equimolar solutions of two sets of nanoprisms functionalized with complementary DNA strands were mixed in a hybridization buffer and heated to 60–65 °C (well above $T_m \approx$ 41 °C of the DNA strands), prisms assembled in a face-to-face manner leading to the formation of 1D crystals with a length varying from 500 nm to 1.2 μm and consisting of 20–40 monomer units, as shown in Fig. 1. The non-uniformity and size variation of the 1D nanoprism crystal can be attributed to the size disparity of the individual building blocks. Prior theoretical and experimental works have shown that polydispersity in colloid suspensions suppresses the nucleation growth and leads to the formation of different crystallites.[62,63]

The melting temperature (T_m) of the 1D nanoprism stacks was determined by monitoring the change in absorbance at the

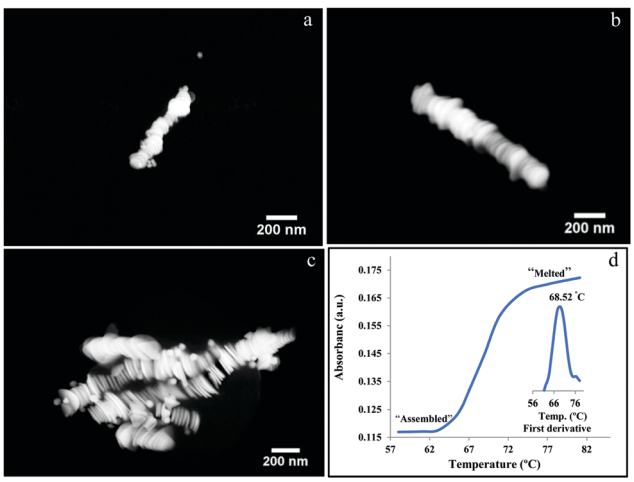

Fig. 1 DNA-mediated face-to-face assembly of gold nanoprisms. (a–c) Representative SEM images of DNA-mediated face-to-face assembly of nanoprisms into 1D stacks, and (d) melting profile of the 1D nanoprism crystals, monitored at the SPR λ_{max} of the nanoprisms. The inset shows the first derivative of the melting curve.

SPR λ_{max} of the nanoprisms as a function of temperature. A control experiment was also carried out by similarly annealing a solution containing uncoated nanoprisms. The melting transition observed for the 1D nanoprism stacks, as shown in Fig. 1d, and the absence of such a profile for thecontrol experiment (Fig. S3, ESI†) indicates that the nanoprisms were densely functionalized with DNA and the melting transition occurred due to the de-hybridization of complementary DNA strands that interconnected the nanoprisms into 1D stacks. The T_m of the 1D nanoprism stacks was found to be 68.5 °C, determined by taking the first derivative of the melting curve and finding the full width of the peak at half maximum (FWHM = 7.2 °C). The melting transition occurred over a relatively broad range, which could be attributed to the dispersity of the 1D nanoprism stacks.

To achieve the long-range ordering and assembly of 1D nanoprism stacks into 3D aggregates, we adopted the near-T_m annealing-based nanoparticle crystallization approach. Thermal annealing is often employed for long-range ordering and crystallization processes in atomic and nanoscale systems.[64,65] Thermal annealing below the T_m of the initially formed DNA-induced amorphous nanoparticle aggregates facilitates particle rearrangement and long-range interaction without aggregate dissociation by reducing the complementary DNA-mediated attraction energy.[59,66]

Prior to thermal annealing below T_m, the solution of 1D nanoprism stacks was spun down and resuspended in 250–300 μL phosphate buffer in order to concentrate the 1D nanoprism stacks, as the organization of 1D nanoprism stacks and crystal growth was not observed for dilute dispersions of stacks even with extended annealing at elevated temperatures. Concentrated dispersions of 1D nanoprism stacks were gradually heated at 65 °C, 66 °C, and 67.5 °C (below $T_m \approx 68.5$ °C) for a period of 1–3 hours (see ESI† for details). Dark-field microscopy was used to characterize the long-range ordering and crystallization of the nanoprisms as thermal treatment progressed.

As illustrated in the dark-field microscopy images, Fig. 2, when thermal annealing was applied, the 1D nanoprism stacks started to hierarchically assemble into 3D aggregates.

As the temperature increased from 55 °C to just below the T_m of the 1D nanoprism stacks, the crystal grain size continued to grow larger. Fig. 2e and Fig. S3 (ESI†) show representative SEM images of the nanoprism aggregates formed below T_m, which are highly polycrystalline with crystal defects and exhibit a size distribution ranging from 5–15 μm in diameter. By contrast, previous studies on the DNA-driven assembly of gold nanoprisms afforded only simple 1D face-to-face stacking.[53,67]

High-magnification SEM images (Fig. 2f and Fig. S3, ESI† insets) allow closer inspection of the 3D polycrystalline nanoprism aggregates, revealing both lateral and perpendicular orientations of 1D nanoprism stacks and the presence of crystal defects within the aggregates. The polycrystallinity of the nanoprism aggregates differs from the well-defined hexagonal or honeycomb aggregates achieved by the salt-mediated crystallization of nanoprisms,[68,69] and predicted by a theoretical study on the phase behavior of polyhedral particles.[70] The lack of well-defined hexagonal or honeycomb aggregates of the nanoprisms could be due to the high polydispersity (around 30–40%) of the nanoprisms used in this study. Mirkin and coworkers showed that having particles (spheres) with a polydispersity less than 10% is crucial for creating DNA-induced well-defined programable crystalline structures.[66]

Close-packed colloidal nanoparticle aggregates give rise to enhanced plasmonic activity.[71,72] We assessed the plasmonic activity of the 3D nanoprism aggregates for applications in surface-enhanced spectroscopies such as surface-enhanced

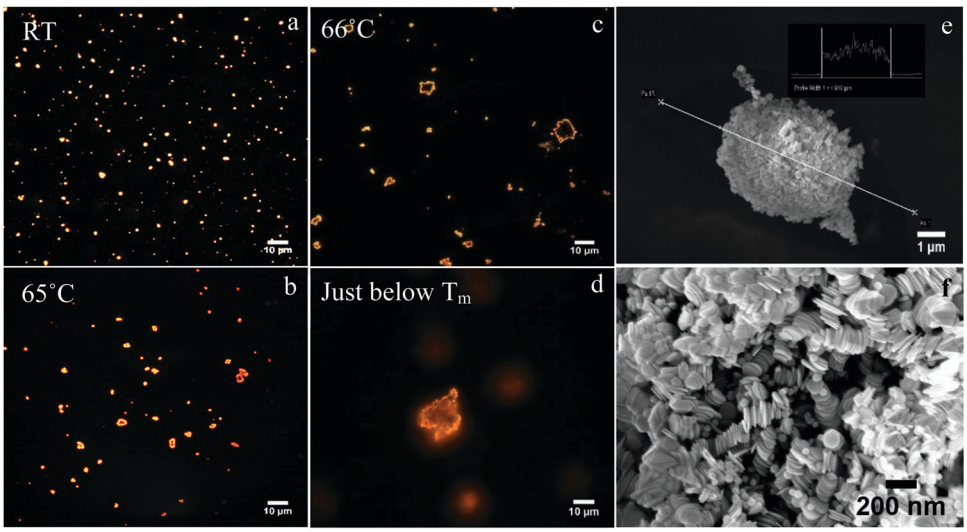

Fig. 2 DNA-mediated 3-D hierarchical organization of gold nanoprisms. Dark-field microscopy images of the long-range ordering of 1D nanoprism stacks at (a) room temperature, (b) 65 °C, (c) 66 °C and (d) just below $T_m \approx 68.5$ °C. (e and f) Representative low- and high-magnification SEM images of the 3D nanoprism aggregates formed below T_m, respectively.

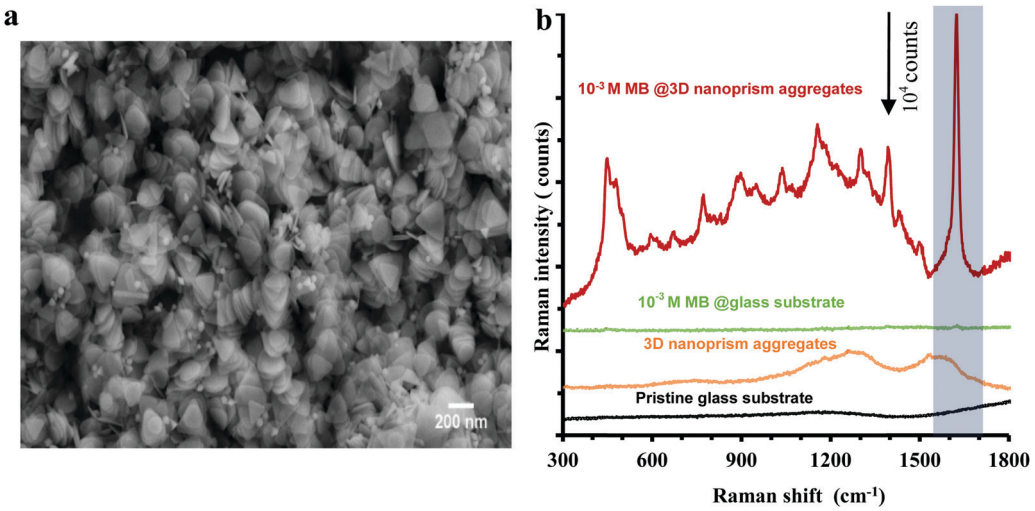

Fig. 3 (a) Representative SEM image of the 3D hierarchical organization of gold nanoprisms on a glass slide and (b) Raman spectra of a pristine glass substrate (black) and the 3D nanoprism aggregates (orange), and SERS spectra of 10^{-3} MB adsorbed on a glass substrate (green) and the 3D nanoprism aggregates (dark red).

Raman scattering (SERS). The SERS enhancement performance of 3D nanoprism aggregates was studied *via* the SERS analysis of methylene blue (MB) as a model compound. MB was chosen as the model compound for SERS analysis because of its well-known characteristic Raman bands. Prior to Raman analysis, the nanoprism aggregate substrate was deposited on a glass slide. The organization of the nanoprisms remained unchanged after drop-casting on glass substrates followed by air-drying, as shown in the SEM image, Fig. 3a. All Raman analyses were carried out on clean silica glass slides under the same experimental conditions, using an excitation wavelength of 633 nm.

Fig. 3b shows the Raman spectra of a bare glass substrate, bare nanoprism aggregates, and 10^{-3} M MB on a glass substrate and on 3D nanoprism aggregates. The Raman spectrum recorded for 10^{-3} M MB on the nanoprism aggregates reveals strong Raman peaks with a good signal-to-noise ratio and characteristics peak positions of MB that are consistent with previous reports.[73–75] Some of the most prominent bands in the SERS spectra of MB are identified at 1621 cm^{-1} for (C–C) ring stretching, 1394 cm^{-1} for (C–N) symmetrical stretching, 1298 cm^{-1} (C–H) in-plane ring deformation, 1154 cm^{-1} for (C–H) in-plane bending, and 449 cm^{-1} for the (C–N–C) skeletal deformation mode. These peaks were not observed in the Raman spectra of the nanoprism aggregates and the glass substrate without MB, indicating that these SERS signals belong to the probe molecule.

While the Raman analysis of 10^{-3} M MB on the 3D nanoprism aggregates reveals a highly structured spectrum with well-defined characteristic peaks of MB, only two peaks with weak intensities were observed at 1621 cm^{-1} and at 450 cm^{-1} for the same concentration of MB using the glass substrate, indicating that the 3D nanoprism substrate is highly SERS-active. The significant enhancement in Raman intensity for the band at 1621 cm^{-1} indicates a favorable orientation and adsorption of the probe molecules to the nanoprisms' surface.[76] The strong SERS enhancement for the 3D substrates is attributed to the presence of the 3D close-packed organization of nanoprism columnar arrays, which facilitates tip-to-tip, tip-to-edge, and edge-to-edge interactions between neighboring nanoprisms and multipolar plasmonic hybridization, leading to the formation of large ensemble plasmonic hot spots, whereas plasmonic coupling between nanoprisms in 1D face-to-face orientations is significantly weaker.[77–79]

To determine the molecular detection limit of the 3D nanoprism aggregates, the SERS spectra for a series of concentrations of MB were collected. Fig. 4a shows the SERS analysis of MB at different concentrations ranging from 10^{-5} to 10^{-10} M. As expected, the intensity of the SERS peaks for MB gradually dropped as the concentration of MB was decreased from 10^{-5} to 10^{-10} M.

The SERS spectra show an obvious peak at 1621 cm^{-1} for the very low MB concentration of 10^{-9} M, indicating that the 3D nanoprism substrate is highly sensitive.

The SERS enhancement factor (EF) of the 3D nanoprism aggregates was calculated from the SERS intensity of the prominent band at 1621 cm^{-1} (10^{-9} M MB) and the Raman intensity of the corresponding band (10^{-3} M MB), considering the bare glass substrate as the reference (see ESI† for details). The SERS EF value of the 3D nanoprism aggregates was estimated to be around 3×10^6. We observed a similar SERS enhancement for another Raman reporter (rhodamine B) using 3D nanoprism aggregates, Fig. S5 (ESI†). By contrast, the 1D array of nanoprisms exhibits a significantly weaker SERS enhancement, Fig. S6 (ESI†). These results are comparable to or better than those of other nanoparticle-based plasmonic SERS substrates for the SERS analysis of MB.[74,75,80–82]

In order to assess the reliability and reproducibility of the 3D nanoprism aggregates as SERS substrates, we adopted a statistical approach to quantify the variation in the SERS response between different samples. To determine the sample-to-sample variation, SERS measurements were recorded for 5 different samples, and for each sample, the signal intensity at 1621 cm^{-1}

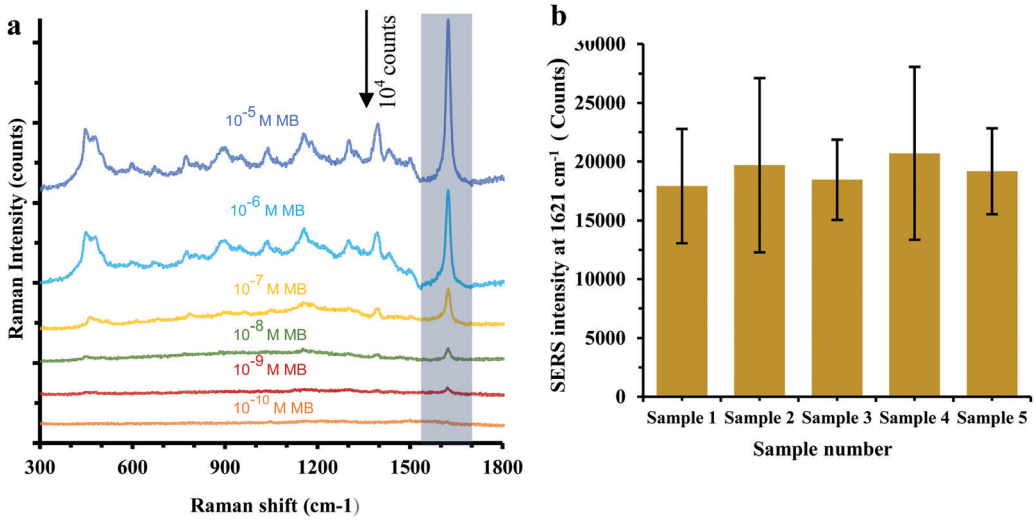

Fig. 4 (a) SERS spectra of MB on 3D nanoprism aggregates at different concentrations, and (b) sample-to-sample SERS intensity variation at 1621 cm^{-1} recorded from 5 different substrates. Error bars represent standard deviations of SERS intensity at 1621 cm^{-1} from at least 6 spots.

was measured from at least 6 different spots. Fig. 4b shows sample-to-sample variation in the average SERS counts at the 1621 cm^{-1} band across 5 different samples. The average signal intensity across the 5 samples was 19 194 counts with a coefficient of variation (CV) of only 5.6%, indicating the excellent reproducibility of the 3D nanoprism aggregates as SERS substrates.

3. Conclusion

In summary, we have demonstrated a DNA-mediated hierarchical assembly of polydisperse gold nanoprisms into 3D aggregates. DNA-functionalized nanoprisms were first assembled into 1D columnar stacks of nanoprisms. Thermal annealing below the T_m of the 1D nanoprism stacks facilitated long-range interactions between the 1D nanoprism stacks and therefore assembly into 3D aggregates with sizes ranging from 5–15 μm in diameter. The large number of closely arranged nanoprism arrays in the 3D crystal led to the formation of an ensemble of plasmonic hot spots, which gave rise to significant enhancement in the SERS signal. SERS analysis of the probe molecule methylene blue, using a 3D nanoprism substrate, showed a significant enhancement ($<10^6$), a high detection sensitivity (as low as 10^{-9}M), and excellent reproducibility. These findings demonstrate that 3D aggregates of anisotropic nanoparticles could find applications in diverse fields such as photonics, chemical sensing, lasing, and nano-plasmonic waveguides.

Conflicts of interest

The authors declare no competing financial interests.

References

1 N. A. Hatab, C.-H. Hsueh, A. L. Gaddis, S. T. Retterer, J.-H. Li, G. Eres, Z. Zhang and B. Gu, Free-Standing Optical Gold Bowtie Nanoantenna with Variable Gap Size for Enhanced Raman Spectroscopy, *Nano Lett.*, 2010, **10**(12), 4952–4955.
2 A. S. M. Z. Kausar, A. W. Reza, T. A. Latef, M. H. Ullah and M. E. Karim, Optical nano antennas: state of the art, scope and challenges as a biosensor along with human exposure to nano-toxicology, *Sensors*, 2015, **15**(4), 8787–8831.
3 K. M. Mayer and J. H. Hafner, Localized Surface Plasmon Resonance Sensors, *Chem. Rev.*, 2011, **111**(6), 3828–3857.
4 J. F. Masson, Surface Plasmon Resonance Clinical Biosensors for Medical Diagnostics, *ACS Sens.*, 2017, **2**(1), 16–30.
5 D. Patel, K. T. James, M. O'Toole, G. Zhang, R. S. Keynton and A. M. Gobin, A high yield, one-pot dialysis-based process for self-assembly of near infrared absorbing gold nanoparticles, *J. Colloid Interface Sci.*, 2015, **441**, 10–16.
6 J. Wang, M. G. O'Toole, A. Massey, S. Biswas, M. Nantz, S. Achilefu and K. Kang, Highly specific, NIR fluorescent contrast agent with emission controlled by gold nanoparticle, *Oxygen Transport to Tissue XXXII*, 2011, pp. 149–154.
7 D. K. Gramotnev and S. I. Bozhevolnyi, Plasmonics beyond the diffraction limit, *Nat. Photonics*, 2010, **4**(2), 83–91.
8 G. Demirel, Surface-enhanced Raman spectroscopy (SERS): an adventure from plasmonic metals to organic semiconductors as SERS platform, *J. Mater. Chem. C*, 2018, **6**(20), 5314–5335.
9 M. Pilo-Pais, A. Watson, S. Demers, T. H. LaBean and G. Finkelstein, Surface-Enhanced Raman Scattering Plasmonic Enhancement Using DNA Origami-Based Complex Metallic Nanostructures, *Nano Lett.*, 2014, **14**(4), 2099–2104.
10 J. Reguera, J. Langer, D. Jimenez de Aberasturi and L. M. Liz-Marzan, Anisotropic metal nanoparticles for surface enhanced Raman scattering, *Chem. Soc. Rev.*, 2017, **46**(13), 3866–3885.
11 J.-F. Li, C.-Y. Li and R. F. Aroca, Plasmon-enhanced fluorescence spectroscopy, *Chem. Soc. Rev.*, 2017, **46**(13), 3962–3979.
12 A. Puchkova, C. Vietz, E. Pibiri, B. Wünsch, M. Sanz Paz, G. P. Acuna and P. Tinnefeld, DNA Origami Nanoantennas

with over 5000-fold Fluorescence Enhancement and Single-Molecule Detection at 25 μM, *Nano Lett.*, 2015, **15**(12), 8354–8359.

13 P. C. Ray, Size and shape dependent second order nonlinear optical properties of nanomaterials and their application in biological and chemical sensing, *Chem. Rev.*, 2010, **110**(9), 5332–5365.

14 M. Yilmaz, E. Senlik, E. Biskin, M. S. Yavuz, U. Tamer and G. Demirel, Combining 3-D plasmonic gold nanorod arrays with colloidal nanoparticles as a versatile concept for reliable, sensitive, and selective molecular detection by SERS, *Phys. Chem. Chem. Phys.*, 2014, **16**(12), 5563–5570.

15 C. Y. Zheng, E. Palacios, W. Zhou, W. Hadibrata, L. Sun, Z. Huang, G. C. Schatz, K. Aydin and C. A. Mirkin, Tunable Fluorescence from Dye-Modified DNA-Assembled Plasmonic Nanocube Arrays, *Adv. Mater.*, 2019, **31**(41), 1904448.

16 J.-E. Park, J. Kim and J.-M. Nam, Emerging plasmonic nanostructures for controlling and enhancing photoluminescence, *Chem. Sci.*, 2017, **8**(7), 4696–4704.

17 X. Chen, C. Jiang and S. Yu, Nanostructured materials for applications in surface-enhanced Raman scattering, *CrystEngComm*, 2014, **16**(43), 9959–9973.

18 L. Scarabelli, M. Coronado-Puchau, J. J. Giner-Casares, J. Langer and L. M. Liz-Marzán, Monodisperse Gold Nanotriangles: Size Control, Large-Scale Self-Assembly, and Performance in Surface-Enhanced Raman Scattering, *ACS Nano*, 2014, **8**(6), 5833–5842.

19 T. Brann, D. Patel, R. Chauhan, K. T. James, P. J. Bates, M. T. Malik, R. S. Keynton and M. G. O'Toole, Gold Nanoplates as Cancer-Targeted Photothermal Actuators for Drug Delivery and Triggered Release, *J. Nanomater.*, 2016, **2016**, 2036029.

20 D.-K. Lim, K.-S. Jeon, H. M. Kim, J.-M. Nam and Y. D. Suh, Nanogap-engineerable Raman-active nanodumbbells for single-molecule detection, *Nat. Mater.*, 2010, **9**(1), 60–67.

21 H. Wei and H. Xu, Hot spots in different metal nanostructures for plasmon-enhanced Raman spectroscopy, *Nanoscale*, 2013, **5**(22), 10794–10805.

22 J. R. Lakowicz, C. D. Geddes, I. Gryczynski, J. Malicka, Z. Gryczynski, K. Aslan, J. Lukomska, E. Matveeva, J. Zhang, R. Badugu and J. Huang, Advances in surface-enhanced fluorescence, *J. Fluoresc.*, 2004, **14**(4), 425–441.

23 H.-Y. Chen, M.-H. Lin, C.-Y. Wang, Y.-M. Chang and S. Gwo, Large-Scale Hot Spot Engineering for Quantitative SERS at the Single-Molecule Scale, *J. Am. Chem. Soc.*, 2015, **137**(42), 13698–13705.

24 Y. Zheng, T. Thai, P. Reineck, L. Qiu, Y. Guo and U. Bach, DNA-Directed Self-Assembly of Core-Satellite Plasmonic Nanostructures: A Highly Sensitive and Reproducible Near-IR SERS Sensor, *Adv. Funct. Mater.*, 2013, **23**(12), 1519–1526.

25 S. Kasani, K. Curtin and N. Wu, A review of 2D and 3D plasmonic nanostructure array patterns: fabrication, light management and sensing applications, *Nanophotonics*, 2019, **8**(12), 2065.

26 H. K. Lee, Y. H. Lee, C. S. L. Koh, G. C. Phan-Quang, X. Han, C. L. Lay, H. Y. F. Sim, Y.-C. Kao, Q. An and X. Y. Ling, Designing surface-enhanced Raman scattering (SERS) platforms beyond hotspot engineering: emerging opportunities in analyte manipulations and hybrid materials, *Chem. Soc. Rev.*, 2019, **48**(3), 731–756.

27 K. J. Si, Y. Chen, Q. Shi and W. Cheng, Nanoparticle Superlattices: The Roles of Soft Ligands, *Adv. Sci.*, 2018, **5**(1), 1700179.

28 A. Dutta, J. Chakraborty, B. L. V. Prasad and P. Sahu, Synthesis and in situ observation of 3D Superlattices of gold nanoparticles using oil-in-water emulsion, *J. Colloid Interface Sci.*, 2014, **420**, 41–49.

29 M. B. Ross, J. C. Ku, V. M. Vaccarezza, G. C. Schatz and C. A. Mirkin, Nanoscale form dictates mesoscale function in plasmonic DNA–nanoparticle superlattices, *Nat. Nanotechnol.*, 2015, **10**(5), 453–458.

30 H. Alaeian and J. A. Dionne, Plasmon nanoparticle superlattices as optical-frequency magnetic metamaterials, *Opt. Express*, 2012, **20**(14), 15781–15796.

31 D. Wang, A. Yang, A. J. Hryn, G. C. Schatz and T. W. Odom, Superlattice Plasmons in Hierarchical Au Nanoparticle Arrays, *ACS Photonics*, 2015, **2**(12), 1789–1794.

32 J. Chen, L. Guo, B. Qiu, Z. Lin and T. Wang, Application of ordered nanoparticle self-assemblies in surface-enhanced spectroscopy, *Mater. Chem. Front.*, 2018, **2**(5), 835–860.

33 W. Wang, M. Ramezani, A. I. Väkeväinen, P. Törmä, J. G. Rivas and T. W. Odom, The rich photonic world of plasmonic nanoparticle arrays, *Mater. Today*, 2018, **21**(3), 303–314.

34 Z. Nie, A. Petukhova and E. Kumacheva, Properties and emerging applications of self-assembled structures made from inorganic nanoparticles, *Nat. Nanotechnol.*, 2010, **5**(1), 15–25.

35 F. Schulz, O. Pavelka, F. Lehmkühler, F. Westermeier, Y. Okamura, N. S. Mueller, S. Reich and H. Lange, Structural order in plasmonic superlattices, *Nat. Commun.*, 2020, **11**(1), 3821.

36 A. Tao, P. Sinsermsuksakul and P. Yang, Tunable plasmonic lattices of silver nanocrystals, *Nat. Nanotechnol.*, 2007, **2**(7), 435–440.

37 P. M. Mendes, S. Jacke, K. Critchley, J. Plaza, Y. Chen, K. Nikitin, R. E. Palmer, J. A. Preece, S. D. Evans and D. Fitzmaurice, Gold Nanoparticle Patterning of Silicon Wafers Using Chemical e-Beam Lithography, *Langmuir*, 2004, **20**(9), 3766–3768.

38 M. H. V. Werts, M. Lambert, J.-P. Bourgoin and M. Brust, Nanometer Scale Patterning of Langmuir−Blodgett Films of Gold Nanoparticles by Electron Beam Lithography, *Nano Lett.*, 2002, **2**(1), 43–47.

39 A. R. Tao, J. Huang and P. Yang, Langmuir-Blodgettry of nanocrystals and nanowires, *Acc. Chem. Res.*, 2008, **41**(12), 1662–1673.

40 P. Li, Y. Li, Z.-K. Zhou, S. Tang, X.-F. Yu, S. Xiao, Z. Wu, Q. Xiao, Y. Zhao, H. Wang and P. K. Chu, Evaporative Self-Assembly of Gold Nanorods into Macroscopic 3D Plasmonic Superlattice Arrays, *Adv. Mater.*, 2016, **28**(13), 2511–2517.

41 W. Wei, Y. Wang, J. Ji, S. Zuo, W. Li, F. Bai and H. Fan, Fabrication of Large-Area Arrays of Vertically Aligned Gold Nanorods, *Nano Lett.*, 2018, **18**(7), 4467–4472.

42 J. Pang, S. Xiong, F. Jaeckel, Z. Sun, D. Dunphy and C. J. Brinker, Free-Standing, Patternable Nanoparticle/Polymer Monolayer Arrays Formed by Evaporation Induced Self-Assembly at a Fluid Interface, *J. Am. Chem. Soc.*, 2008, **130**(11), 3284–3285.
43 Q. Shi, W. Di, D. Dong, L. W. Yap, L. Li, D. Zang and W. Cheng, A General Approach to Free-Standing Nanoassemblies via Acoustic Levitation Self-Assembly, *ACS Nano*, 2019, **13**(5), 5243–5250.
44 J. Ou, H. Tan, X. Chen and Z. Chen, DNA-Assisted Assembly of Gold Nanostructures and Their Induced Optical Properties, *Nanomaterials*, 2018, **8**(12), 994.
45 B. Radha, A. J. Senesi, M. N. O'Brien, M. X. Wang, E. Auyeung, B. Lee and C. A. Mirkin, Reconstitutable Nanoparticle Superlattices, *Nano Lett.*, 2014, **14**(4), 2162–2167.
46 A. P. Alivisatos, K. P. Johnsson, X. Peng, T. E. Wilson, C. J. Loweth, M. P. Bruchez and P. G. Schultz, Organization of 'nanocrystal molecules' using DNA, *Nature*, 1996, **382**(6592), 609–611.
47 R. R. Mazid, K. J. Si and W. Cheng, DNA based strategy to nanoparticle superlattices, *Methods*, 2014, **67**(2), 215–226.
48 A. Kumar, J.-H. Hwang, S. Kumar and J.-M. Nam, Tuning and assembling metal nanostructures with DNA, *Chem. Commun.*, 2013, **49**(26), 2597–2609.
49 S. J. Tan, M. J. Campolongo, D. Luo and W. Cheng, Building plasmonic nanostructures with DNA, *Nat. Nanotechnol.*, 2011, **6**(5), 268–276.
50 M. Girard; J. A. Millan and M. O. de la Cruz, DNA-Driven Assembly: From Polyhedral Nanoparticles to Proteins, in *Annual Review of Materials Research*, ed. D. R. Clarke, 2017, vol. 47, pp. 33–49.
51 Y. Zhang, F. Lu, K. G. Yager, D. van der Lelie and O. Gang, A general strategy for the DNA-mediated self-assembly of functional nanoparticles into heterogeneous systems, *Nat. Nanotechnol.*, 2013, **8**(11), 865–872.
52 K. L. Young, M. B. Ross, M. G. Blaber, M. Rycenga, M. R. Jones, C. Zhang, A. J. Senesi, B. Lee, G. C. Schatz and C. A. Mirkin, Using DNA to Design Plasmonic Metamaterials with Tunable Optical Properties, *Adv. Mater.*, 2014, **26**(4), 653–659.
53 M. R. Jones, R. J. Macfarlane, B. Lee, J. Zhang, K. L. Young, A. J. Senesi and C. A. Mirkin, DNA-nanoparticle superlattices formed from anisotropic building blocks, *Nat. Mater.*, 2010, **9**(11), 913–917.
54 F. Lu, K. G. Yager, Y. Zhang, H. Xin and O. Gang, Superlattices assembled through shape-induced directional binding, *Nat. Commun.*, 2015, **6**, 6912.
55 M. N. O'Brien, M. R. Jones, B. Lee and C. A. Mirkin, Anisotropic nanoparticle complementarity in DNA-mediated cocrystallization, *Nat. Mater.*, 2015, **14**(8), 833–839.
56 E. Chowdhury, C. A. Grapperhaus and M. G. O'Toole, Facet-selective asymmetric functionalization of anisotropic gold nanoprisms for Janus particle synthesis, *J. Nanopart. Res.*, 2020, **22**(6), 142.
57 K. T. James, M. G. O'Toole, D. N. Patel, G. Zhang, A. M. Gobin and R. S. Keynton, A high yield, one-pot dialysis-based process for self-assembly of near infrared absorbing gold nanoparticles, *J. Colloid Interface Sci.*, 2015, **441**, 10–16.
58 X. Li, X. Liu and X. Liu, Self-assembly of colloidal inorganic nanocrystals: nanoscale forces, emergent properties and applications, *Chem. Soc. Rev.*, 2021, **50**(3), 2074–2101.
59 D. Nykypanchuk, M. M. Maye, D. van der Lelie and O. Gang, DNA-guided crystallization of colloidal nanoparticles, *Nature*, 2008, **451**(7178), 549–552.
60 J. S. Kahn, B. Minevich and O. Gang, Three-dimensional DNA-programmable nanoparticle superlattices, *Curr. Opin. Biotechnol*, 2020, **63**, 142–150.
61 F. Lu, T. Vo, Y. Zhang, A. Frenkel, K. G. Yager, S. Kumar and O. Gang, Unusual packing of soft-shelled nanocubes, *Sci. Adv.*, 2019, **5**(5), eaaw2399.
62 S. Auer and D. Frenkel, Suppression of crystal nucleation in polydisperse colloids due to increase of the surface free energy, *Nature*, 2001, **413**(6857), 711–713.
63 C. L. Phillips and S. C. Glotzer, Effect of nanoparticle polydispersity on the self-assembly of polymer tethered nanospheres, *J. Chem. Phys.*, 2012, **137**(10), 104901.
64 C. R. Laramy, M. N. O'Brien and C. A. Mirkin, Crystal engineering with DNA, *Nat. Rev. Mater.*, 2019, **4**(3), 201–224.
65 S. Lan, C. Guo, W. Zhou, Y. Ren, J. Almer, C. Pei, H. Hahn, C.-T. Liu, T. Feng, X.-L. Wang and H. Gleiter, Engineering medium-range order and polyamorphism in a nanostructured amorphous alloy, *Commun. Phys.*, 2019, **2**(1), 117.
66 S. Y. Park, A. K. R. Lytton-Jean, B. Lee, S. Weigand, G. C. Schatz and C. A. Mirkin, DNA-programmable nanoparticle crystallization, *Nature*, 2008, **451**(7178), 553–556.
67 S. S. Sinha, S. Jones, T. Demeritte, S. R. Chavva, Y. Shi, J. Burrell, A. Pramanik and P. C. Ray, Multimodal Nonlinear Optical Imaging of Live Cells Using Plasmon-Coupled DNA-Mediated Gold Nanoprism Assembly, *J. Phys. Chem. C*, 2016, **120**(8), 4546–4555.
68 B. Luo, A. Kim, J. W. Smith, Z. Ou, Z. Wu, J. Kim and Q. Chen, Hierarchical self-assembly of 3D lattices from polydisperse anisometric colloids, *Nat. Commun.*, 2019, **10**(1), 1815.
69 Z. Ou, Z. Wang, B. Luo, E. Luijten and Q. Chen, Kinetic pathways of crystallization at the nanoscale, *Nat. Mater.*, 2020, **19**(4), 450–455.
70 U. Agarwal and F. A. Escobedo, Mesophase behaviour of polyhedral particles, *Nat. Mater.*, 2011, **10**(3), 230–235.
71 J. Yoon, H.-J. Jang, I. Jung and S. Park, A close-packed 3D plasmonic superlattice of truncated octahedral gold nanoframes, *Nanoscale*, 2017, **9**(23), 7708–7713.
72 C. Matricardi, C. Hanske, J. L. Garcia-Pomar, J. Langer, A. Mihi and L. M. Liz-Marzán, Gold Nanoparticle Plasmonic Superlattices as Surface-Enhanced Raman Spectroscopy Substrates, *ACS Nano*, 2018, **12**(8), 8531–8539.
73 G. Demirel, R. L. M. Gieseking, R. Ozdemir, S. Kahmann, M. A. Loi, G. C. Schatz, A. Facchetti and H. Usta, Molecular engineering of organic semiconductors enables noble metal-comparable SERS enhancement and sensitivity, *Nat. Commun.*, 2019, **10**(1), 5502.

74 C. Li, Y. Huang, K. Lai, B. A. Rasco and Y. Fan, Analysis of trace methylene blue in fish muscles using ultra-sensitive surface-enhanced Raman spectroscopy, *Food Control*, 2016, **65**, 99–105.
75 T. Xu, X. Wang, Y. Huang, K. Lai and Y. Fan, Rapid detection of trace methylene blue and malachite green in four fish tissues by ultra-sensitive surface-enhanced Raman spectroscopy coated with gold nanorods, *Food Control*, 2019, **106**, 106720.
76 S. D. Roy, M. Ghosh and J. Chowdhury, Adsorptive parameters and influence of hot geometries on the SER(R)S spectra of methylene blue molecules adsorbed on gold nanocolloidal particles, *J. Raman Spectrosc.*, 2015, **46**(5), 451–461.
77 E. Chowdhury, M. S. Rahaman, N. Sathitsuksanoh, C. A. Grapperhaus and M. G. O'Toole, DNA-induced assembly of gold nanoprisms and polystyrene beads into 3D plasmonic SERS substrates, *Nanotechnology*, 2020, **32**(2), 025506.
78 M. Kotkowiak, B. Grześkiewicz, E. Robak and E. Wolarz, Interaction between Nanoprisms with Different Coupling Strength, *J. Phys. Chem. C*, 2015, **119**(11), 6195–6203.
79 N. Hooshmand, J. A. Bordley and M. A. El-Sayed, The Sensitivity of the Distance Dependent Plasmonic Coupling between Two Nanocubes to their Orientation: Edge-to-Edge versus Face-to-Face, *J. Phys. Chem. C*, 2016, **120**(8), 4564–4570.
80 C. Srichan, M. Ekpanyapong, M. Horprathum, P. Eiamchai, N. Nuntawong, D. Phokharatkul, P. Danvirutai, E. Bohez, A. Wisitsoraat and A. Tuantranont, Highly-Sensitive Surface-Enhanced Raman Spectroscopy (SERS)-based Chemical Sensor using 3D Graphene Foam Decorated with Silver Nanoparticles as SERS substrate, *Sci. Rep.*, 2016, **6**(1), 23733.
81 M. Yilmaz, Combining 3-D plasmonic gold nanorod arrays with colloidal nanoparticles as a versatile concept for reliable, sensitive, and selective molecular detection by SERS, *Phys. Chem. Chem. Phys.*, 2014, **16**(12), 5563–5570.
82 G.-N. Xiao and S.-Q. Man, Surface-enhanced Raman scattering of methylene blue adsorbed on cap-shaped silver nanoparticles, *Chem. Phys. Lett.*, 2007, **447**(4), 305–309.